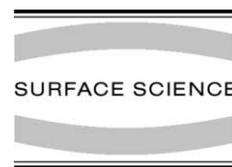




ELSEVIER

Surface Science 476 (2001) 22–34



www.elsevier.nl/locate/susc

Morphology and electronic structure of the Ca/Si(1 1 1) system

A.A. Baski^{a,*}, S.C. Erwin^b, M.S. Turner^a, K.M. Jones^a, J.W. Dickinson^a,
J.A. Carlisle^c

^a Department of Physics, Virginia Commonwealth University, 1020 W. Main Street, Richmond, VA 23284, USA

^b Center for Computational Materials Science, Naval Research Laboratory, Washington, DC 20375, USA

^c Materials Science Division, Argonne National Laboratory, Argonne, IL 60439, USA

Received 24 October 2000; accepted for publication 14 December 2000

Abstract

The Ca/Si(1 1 1) system has been studied using reflection high-energy electron diffraction, scanning tunneling microscopy (STM), synchrotron radiation photoemission, and first-principles total-energy calculations. This system forms a series of odd-order $n \times 1$ ($n = 3, 5, 7, \dots$) reconstructions that culminate with a 2×1 phase at 0.5 ML. Our results indicate that the honeycomb-chain-channel (HCC) model accounts well for the observed data from the 3×1 surface. We propose a model for the 2×1 phase based upon π -bonded Seiwatz Si chains, and explain the intermediate odd-order phases as appropriate combinations of the 2×1 Seiwatz chains and 3×1 HCC chains. Calculated surface energies based on this model correctly predict that for increasing Ca coverage, the 3×1 , 5×1 , and 2×1 phases will each appear as stable phases. Simulated STM images are in excellent agreement with experiment. The Ca 3×1 phase exhibits a suppression of emission at the Fermi level and a local $2a$ ($a = 0.38$ nm) corrugation along the rows in STM images, both of which are consistent with the formation of either a charge-density wave or a one-dimensional correlated insulator. © 2001 Elsevier Science B.V. All rights reserved.

Keywords: Alkaline earth metals; Silicon; Reflection high-energy electron diffraction (RHEED); Scanning tunneling microscopy; Synchrotron radiation photoelectron spectroscopy; Density functional calculations; Electron density, excitation spectra calculations; Surface relaxation and reconstruction

1. Introduction

The electronic properties of surfaces with one-dimensional (1D) structures have been a subject of intense interest, both fundamentally and as a result of their increased importance in semiconductor devices. In particular, the growth of 1D metallic

structures on semiconducting substrates has yielded a number of systems that exhibit interesting electronic properties [1–5]. Recently, one such system that has attracted strong interest is the row-like growth of alkali and related adsorbates on Si(1 1 1). It is known that Na, Li and Ag form a 3×1 reconstruction at 1/3 ML, where an array of rows with a $3a$ inter-row spacing ($a = 0.38$ nm) is observed via scanning tunneling microscopy (STM) [1–3]. Because these systems demonstrate similar structural and electronic properties, proposed structural models have incorporated a

* Corresponding author. Tel.: +1-804-828-8295; fax: +804-828-7073.

E-mail address: aabaski@vcu.edu (A.A. Baski).

common arrangement of the Si atoms. Most recently, a honeycomb-chain-channel (HCC) model which incorporates Si double bonds was found to be energetically more favorable than other π -bonded chain models [4–7].

In this study, we examine a related group-II system for which few studies exist: Ca/Si(1 1 1). The surface structural and electronic properties are investigated using reflection high-energy electron diffraction (RHEED), STM, synchrotron-radiation photoemission (PES), and first-principles total-energy calculations. This system forms a 3×1 reconstruction similar to the alkali metals; however, it also forms a series of odd-order $n \times 1$ reconstructions that culminate in a 2×1 phase at 0.5 ML. This coverage behavior is similar to that observed for the divalent rare-earth Yb [8,9]. The Ca/Si(1 1 1) system is interesting because these additional reconstructions should be a natural extension of the structural model proposed for the alkali metal 3×1 phase. In fact, our STM results indicate that the Ca 3×1 rows may coexist with 5×1 and 7×1 rows, indicating that they incorporate similar structures. First-principles band structure calculations based on our proposed structural models predict that the 3×1 phase should be metallic and the 2×1 phase semiconducting. However, valence band spectra indicate that all of these phases are semiconducting with no detectable emission near the Fermi level. In addition, we find that the 3×1 reconstruction exhibits a local $2a$ ($a = 0.38$ nm) corrugation along the rows, which combined with the above result is consistent with the formation of either a charge-density wave or a 1D correlated insulator [10].

2. Experiment

The Ca/Si(1 1 1) surface was characterized using RHEED, STM, and PES in three separate ultra-high vacuum (UHV) systems. In all cases, the substrates were n-type Si(1 1 1) and were cleaned by direct heating to $\sim 1200^\circ\text{C}$ for 1–2 min. Calcium deposition was performed using an e-beam evaporator in the RHEED and PES chambers, and using a filament heater in the STM chamber, where the Ca deposition rate was calibrated with a

quartz crystal microbalance in each chamber. Typical rates were 0.1–1 ML/min, with 1 ML equal to the atomic density of the bulk-terminated Si(1 1 1) surface, or 7.8×10^{14} atoms/cm². Ca was deposited onto preheated substrates (RHEED) or onto room temperature substrates that were subsequently annealed (PES and STM). The sample temperature was monitored using the same optical pyrometer in all cases.

The RHEED system was equipped with a Staib 15 kV electron gun and a K-Space Associates data acquisition system. The STM system included low energy electron diffraction (LEED) and an Omicron STM1 instrument. STM images of the filled electronic states were acquired at room temperature with a constant current between 0.15 and 0.5 nA and bias voltages between 1.0 and 2.5 V. The PES measurements were performed at the Synchrotron Radiation Center in Stoughton, WI (SRC) using the University of Illinois photoemission endstation on beamlines 042 and 071.¹ Valence band and core-level spectra were obtained on cooled samples (-172°C) using a large hemispherical analyzer in angle-integrated mode with a 15° acceptance cone. Total instrumental resolution for both the core-level and valence-band data is ~ 50 meV. We analyzed the Si 2p core-level peaks using a standard non-linear, least-squares fitting algorithm. Voigt-line shapes were used with Gaussian and Lorentzian widths of 0.25 and 0.07 eV, respectively.

3. Theory

To characterize the ordered surface phases theoretically, we carried out first-principles total-energy calculations using density-functional theory within the generalized-gradient approximation [11]. Our structural models for the 3×1 , 5×1 , and 2×1 phases (described below) were relaxed within a symmetric slab geometry containing 12 Si layers and a vacuum region of ~ 10 Å. The innermost two Si layers were fixed at their bulk positions,

¹ More information regarding the SRC can be found at <http://www.src.wisc.edu/>.

while all other atoms were relaxed until every force component was smaller than 0.05 eV/\AA . Total energies and forces were calculated using soft pseudopotentials consistently constructed within the generalized-gradient approximation, as implemented in the fhi96md code [12]. The plane-wave energy cutoff was 18 Ry. For each phase, the surface Brillouin zone was sampled at a k-point density sufficient to converge the absolute surface energies to better than 1 meV/\AA^2 . Simulated STM images were then constructed using the Tersoff–Hamann approximation, in which the local density of states (LDOS) is integrated over energies within $E = eV$ of the Fermi level, where V is the tunneling voltage. The topographic map of the height at which the integrated LDOS is constant then simulates the experimental constant-current tunneling image.

We also calculated surface core-level shifts for the 3×1 and 2×1 phases, using both initial-state (IST) and final-state theory (FST) [13]. These two approaches differ primarily in their treatment of the electronic relaxation accompanying the creation of a core hole during the photoemission process: IST assumes no screening of the core hole, whereas FST assumes complete screening. The core-level shifts were determined within IST by calculating the Si atomic 2p expectation value of the Coulomb potential arising from the self-consistent crystalline pseudocharge density. These integrals closely approximate the different Si 2p core eigenvalues that would be found in an all-electron calculation.² Core-level shifts were calculated within FST by first constructing a new pseudopotential with an electron promoted from the 2p to 3p level. This pseudopotential was then used to represent a single excited Si atom within a doubled supercell of the 3×1 or 2×1 phase. The change in total energy for different positions of the excited atom (relative to a bulk-like position) then gives the core-level shifts directly. In general, the FST

shift is equal to the IST shift plus a screening correction due to core-hole relaxation.

4. Results

As the Ca coverage is increased, the Ca/Si(1 1 1) system exhibits at least four distinct $n \times 1$ phases (n odd) before a 2×1 reconstruction is formed at 0.5 ML. All of these reconstructions require the surface to be annealed, where we have found that a temperature of $\approx 550^\circ\text{C}$ yields the sharpest RHEED patterns. Fig. 1(a)–(c) shows RHEED images of the most common phases: 3×1 at $1/3$ ML, 5×1 at $2/5$ ML, and 2×1 at $1/2$ ML. Fig. 1(d) is a time-lapse image obtained by monitoring pixel intensity along the lines shown in (a)–(c). The odd $n \times 1$ phases clearly show an overlap in their transition regions, indicating that these phases may coexist on the surface. When the sample temperature is increased to desorb the Ca, the lowest coverage 3×1 phase is found to have the highest desorption temperature and therefore to be the most stable phase. Note that the background intensity in the RHEED images does not substantially change as the system evolves. If the various reconstructions involved a massive rearrangement of Si atoms, then the background scattering should change dramatically from one phase to the next. We therefore believe that all of these phases involve similar surface structures.

STM data showing the morphology and atomic structure of the lowest coverage 3×1 phase is shown in Fig. 2. In large-scale images, the 3×1 phase appears as striped domains growing adjacent to clean 7×7 regions (see Fig. 2(a)). These domains are composed of stripes oriented in one of three symmetry directions and have a $3a$ ($a = 0.38 \text{ nm}$) inter-row spacing. Two such orientations are shown in the cropped image of Fig. 2(b), where the domain walls appear to be quite abrupt between 120° rotated orientations. The higher resolution, filled-state image of Fig. 2(c) indicates that the stripes composing the 3×1 phase actually consist of paired asymmetric rows. The overall appearance of these rows is similar to that observed for other 3×1 metal systems, indicating that Ca induces a similar reconstruction compared to the

² We use the Coulomb potential (and not the total effective potential) to calculate core-level shifts. This procedure leads to better agreement with all-electron results for the core-level shifts of atomic Si in excited electronic configurations, and so we adopt it here as well [23].

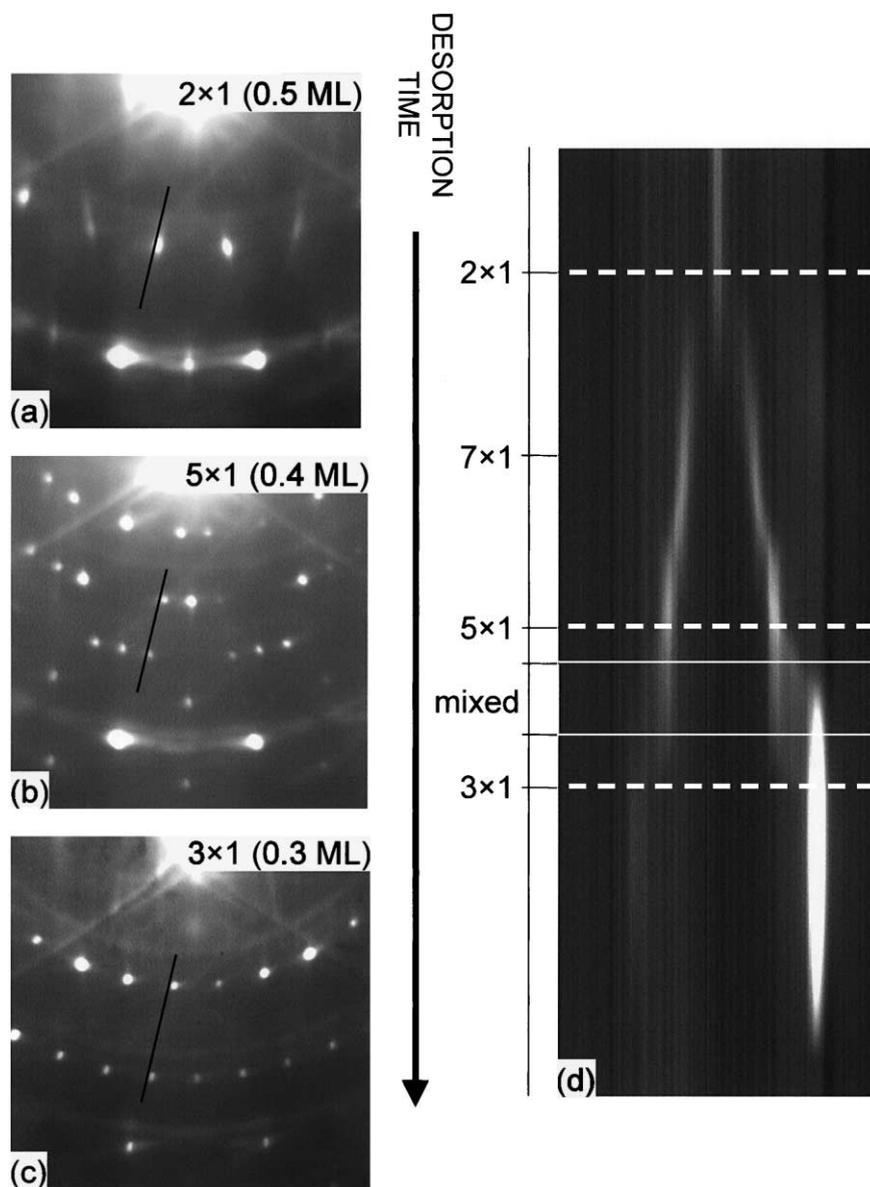


Fig. 1. (a)–(c) Representative RHEED images for the most common $n \times 1$ phases. (d) A “streak” diagram where an image is formed by monitoring the diffraction intensity along the lines indicated in (a)–(c).

alkali metals at this coverage [1–3]. In filled-state images, these paired rows typically have a $1a$ period along the row direction, but frequently develop a local $2a$ period. When this period doubling occurs, the “right” row (towards $\langle 11\bar{2} \rangle$ direction) is composed of prominent round protrusions, whereas the left row shows only a weak pairing of the existing

$1a$ corrugations (see insert). Such $2a$ ordering is also observed in empty-state images (see Fig. 4(b) and (c)). This period doubling along the row direction has not been observed in STM studies of the alkali metal 3×1 systems, but was recently seen in other STM studies of Mg and Ca [14,15]. In the work of Saranin et al. [15] on Ca, 3×2 ordering

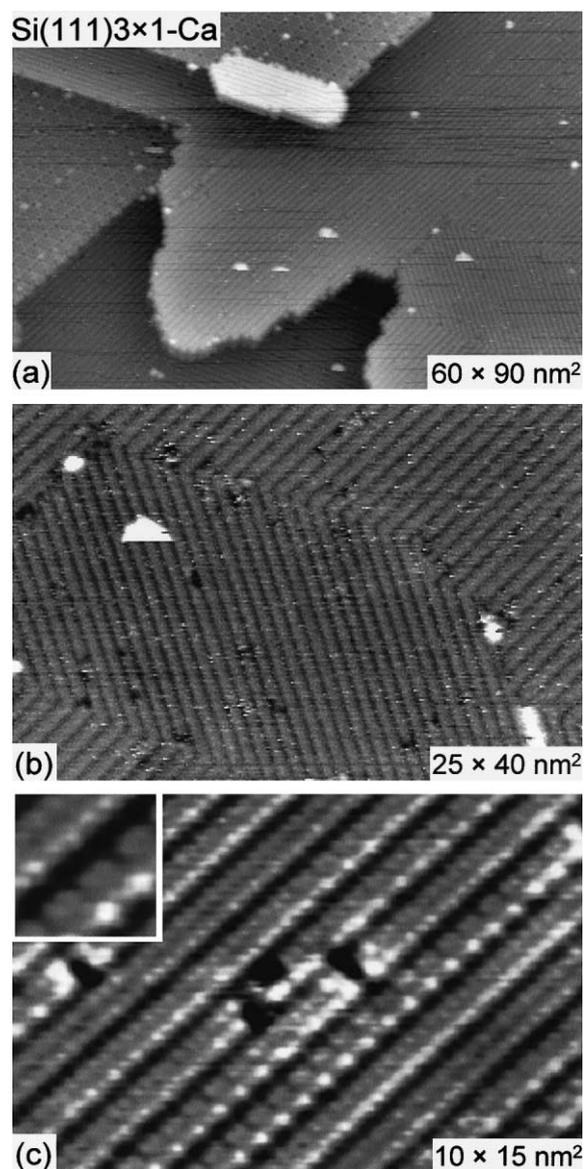


Fig. 2. Filled-state STM images of the Si(111) 3×1 -Ca surface. In (a), clean 7×7 regions are visible adjacent to the striped 3×1 domains, which are seen at higher magnification in (b) and (c). An atomic resolution image in (c) shows the double row structure of this phase, as well as $2a$ ($a = 0.38$ nm) ordering along the row direction (see inset).

was prevalent in empty-state images and resulted in weak half-order LEED streaks. In our extensive RHEED studies, however, we did not detect half-order streaks.

As shown earlier in our RHEED study, Ca forms higher order reconstructions (5×1 , 7×1 , 2×1) at coverages above $1/3$ ML. This behavior distinguishes Ca from the alkali metals, where such reconstructions are not observed. Fig. 3 shows STM images of a mostly 5×1 surface formed at ≈ 0.4 ML coverage, which has been imaged for the first time in this work. The large-scale image in Fig. 3(a) shows that the surface morphology consists of terraces covered by a large number of islands. The presence of such islands is a result of the difference in Si density for the clean 7×7 vs. Ca-induced reconstructions [15]. Both the terraces and islands are composed of striped structures, as seen more clearly in Fig. 3(b). The majority of these stripe structures have a $5a$ width; however, they are occasionally interrupted by stripes with a $7a$ or $3a$ width (see Fig. 3(c)).³ Local mixing of the 3×1 and $n \times 1$ phases, in particular the occurrence of single unit cells (or stripes) of one phase coexisting with another, indicates that the atomic models for these phases should be closely related.

Fig. 4(a) and (b) shows a dual-bias image of this same predominantly 5×1 surface, where 3×1 , 5×1 and 7×1 stripes are present. The filled-state image in Fig. 4(a) shows relatively diffuse structures for all three stripes, where adjacent stripes are separated by dark trenches. Note that in this image the tip resolution is not sufficient to distinguish the paired 3×1 rows. The surface looks somewhat disordered because there are a number of dark localized defects along the 5×1 and 7×1 rows, which usually appear as bright protrusions in the empty electronic states. With regard to the empty states, the 3×1 stripes consist of a single row, whereas the 5×1 (or 7×1) stripes are composed of two (or three) rows. These rows are more clearly visible in Fig. 4(c), which is another empty-state image taken on a different sample with a similar coverage. The single 3×1 row is consistent with other empty-state STM images of related alkali systems, but there is no comparable

³ The coexistence of these phases could be considered a 2D analogue of the phenomenon of intergrowth found for 3D crystals, such as for the Bi2212 and Bi2223 system [24].

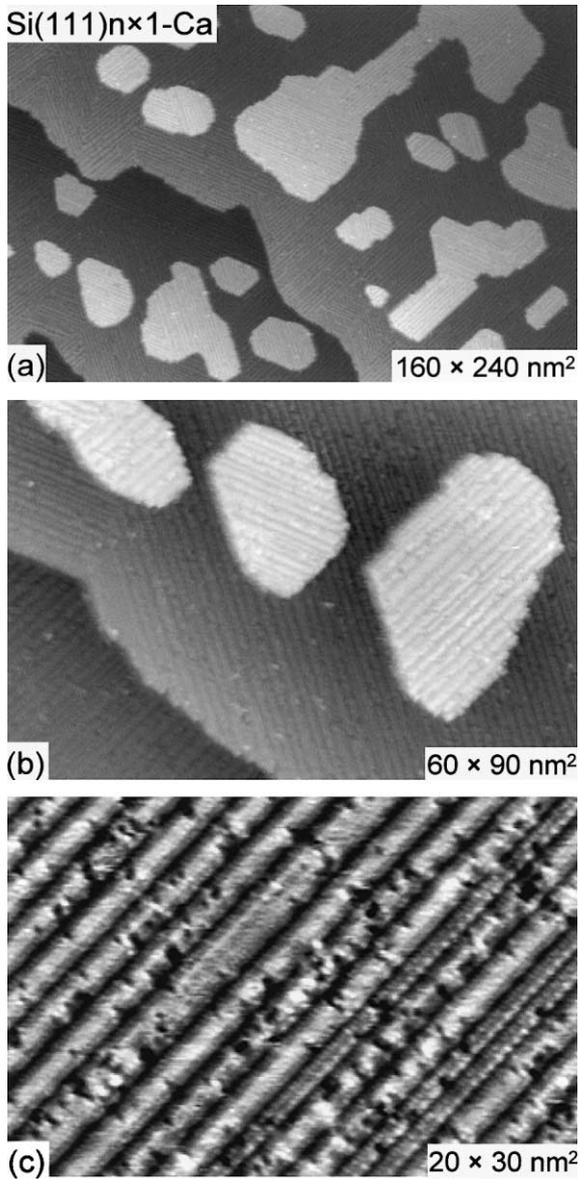


Fig. 3. Filled-state STM images of the mixed Si(111) $n \times 1$ -Ca surface. As shown in (a) and (b), this phase results in terraces and islands composed of striped structures of varying widths. These widths correspond to local 7×1 , 5×1 , and 3×1 unit cells which are intermixed on the surface.

data for the higher order phases. Note that the 3×1 row sometimes has a weak $2a$ corrugation along the row direction, which is not detectable in the filled states (left side of Fig. 4(b) and right side

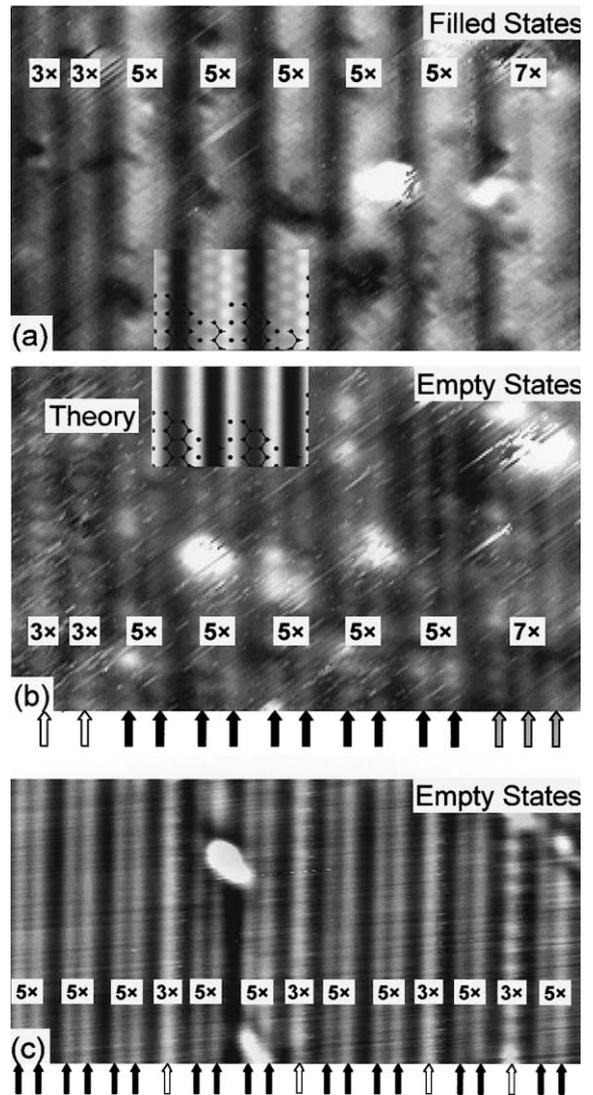


Fig. 4. (a), (b) Dual-bias image of the Si(111) $n \times 1$ -Ca surface shown in Fig. 3, where odd-order $n \times 1$ unit cells are labeled (-2 V filled; 2 V empty). (c) Empty-state image (1 V) of another sample with comparable Ca coverage. The stripes associated with the labeled unit cells show little corrugation in the filled states. In empty-state images, however, such stripes are composed of increasing numbers of row structures, i.e. 1 row for 3×1 , 2 rows for 5×1 , and 3 rows for 7×1 . Simulated STM images based on our proposed model are shown in the insets of (a) and (b).

of Fig. 4(c)). A simulated 5×1 image based upon our proposed model is superimposed on Fig. 4(a) and (b), and will be addressed in Section 5.

The highest coverage 2×1 phase, which has also not been previously observed by STM, is shown in Fig. 5. The larger-scale image in Fig. 5(a) shows a region of the surface containing all three domains of the 2×1 reconstruction. Each domain is composed of stripes which are occasionally interrupted by defect structures, the most prominent being a low density of bright adsorbed features. These protrusions are most likely adsorbed contaminants not intrinsic to the 2×1 surface. In the higher resolution, filled-state image shown in Fig. 5(b), the rows of one 2×1 domain are clearly visible, where one row occurs per 2×1 unit cell. Empty-state images of this surface are similar in appearance and also show row structures with no observable corrugations along their length. Of all of the Ca-induced structures on the Si(111) sur-

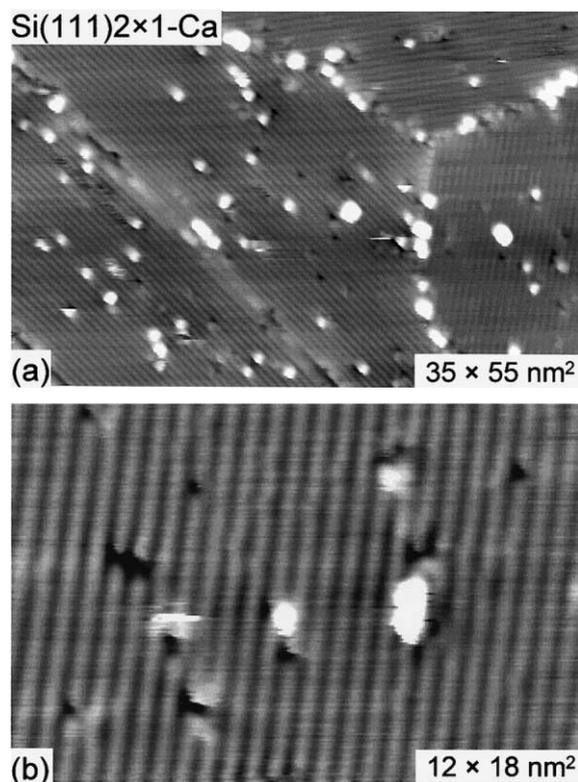


Fig. 5. Filled-state STM images of the Si(111) 2×1 -Ca surface. This phase results in the formation of simple row structures with a $2a$ ($a = 0.38$ nm) inter-row spacing. The bright protrusions are adsorbed defects not intrinsic to the reconstruction.

face, the 2×1 phase has the simplest appearance in both biases.

The electronic structure of the various phases for the Ca/Si(111) systems has also been investigated using photoemission spectroscopy. A sequence of Si 2p core level spectra taken during the desorption of Ca from the Si(111) surface is shown in Fig. 6. In general, while the endpoint 3×1 and 2×1 core-level line shapes appear relatively simple, the line shapes for the intermediate phases are substantially more complex. Similar results have been obtained in the related Yb/Si(111) system [8,9]. Our spectra for the 3×1 phase resemble those observed for the alkali 3×1 systems mentioned earlier, again corroborating the premise that all of the 3×1 reconstructions share a common structure. The 2×1 and 3×1 surfaces

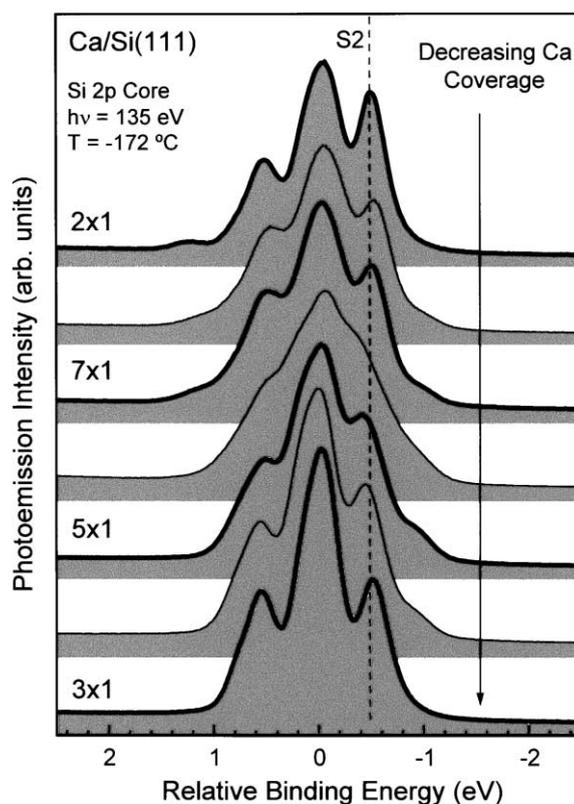


Fig. 6. Evolution of the Si 2p core-level as Ca is desorbed from the surface. The 2×1 and 3×1 spectra appear simpler in appearance in comparison to the intermediate odd-order $n \times 1$ phases.

clearly have similar features, in particular a component shifted to both lower and higher binding energies. Figs. 7 and 8 show the deconvolutions of these component peaks, as well as other minor surface peaks. The larger peak labeled S2 is shifted -0.41 eV to lower binding energy and its intensity relative to the bulk peak B increases with Ca coverage ($\sim 25\%$ increase from the 3×1 to 2×1 phase). In contrast, the smaller peak S1 is shifted $+0.25$ eV to higher binding energy and decreases in intensity with coverage. The calculated surface core-level shifts indicated in Figs. 7 and 8 are discussed in more detail below.

It is natural to associate S2 with Si atoms that interact directly with the Ca atoms at the surface. Due to charge transfer from Ca to Si, the 2p core level associated with these atoms is expected to be shifted to lower binding energy. The intensity of this component should increase with coverage until the 2×1 completion phase is reached, at which point all surface silicon atoms are of the S2

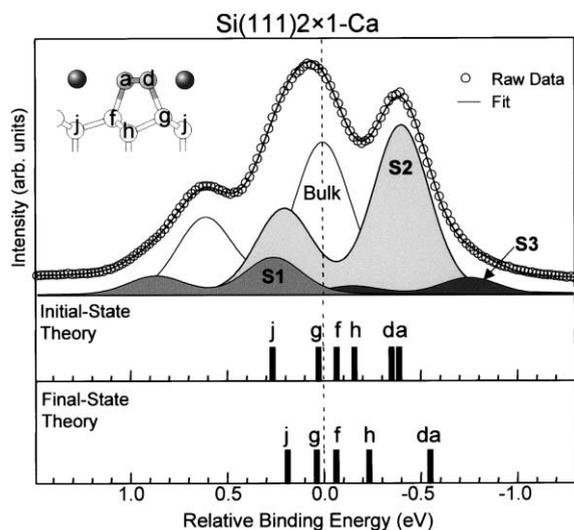


Fig. 7. Si 2p core-level spectra for the 2×1 surface obtained at $h\nu = 135$ eV photon energy and $T = -172^\circ\text{C}$. The open circles are raw data and the solid lines are fits. Also shown are the calculated surface core level binding energies using both initial-state and final-state theory for the different atoms in the proposed 2×1 reconstruction. The inset in the top left is a cross-sectional model for the 2×1 phase based on Seiwatz chains, with the atom labels included for comparison to the calculations.

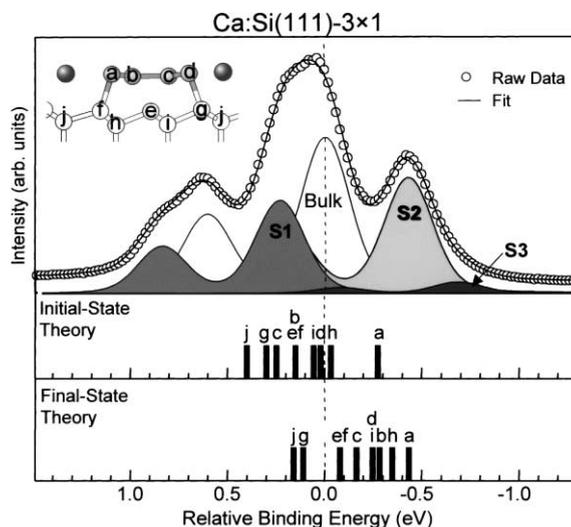


Fig. 8. Si 2p core-level spectra for the 3×1 surface, with identical conditions as described in Fig. 7. The calculated core-level binding energies are also shown, along with a cross-sectional model of the HCC reconstruction. The atoms labels are again included for comparison to the calculations.

type. The intensity of this component relative to the bulk indicates that the number of Si atoms participating in the 2×1 reconstruction is slightly more than one monolayer. An assignment of the S1 peak is more subtle. Many systems exhibit similarly shifted components that are frequently attributed to second-layer Si atoms [16]. It should be noted, however, that calculations by Kang et al. for the $\text{Si}(111)3 \times 1\text{-Na}$ system assign this higher binding energy peak to first-layer, double-bonded Si atoms in the HCC reconstruction [7,17]. Our surface core-level shift calculations for the 3×1 phase do not confirm this assignment, and indicate that second-layer atoms are indeed responsible for the S1 surface core level.

Angle-integrated valence band spectra for the three most common Ca/Si(111) phases and the clean $\text{Si}(111)-(7 \times 7)$ surface are shown in Fig. 9. These spectra are fully integrated over the entire surface Brillouin zone, due to the combination of a 55 eV excitation energy, a three-domain surface and the 15° acceptance cone of the electron energy analyzer. These valence bands are therefore representative of the density of states for the surface. The relatively simple line shape evolution of these

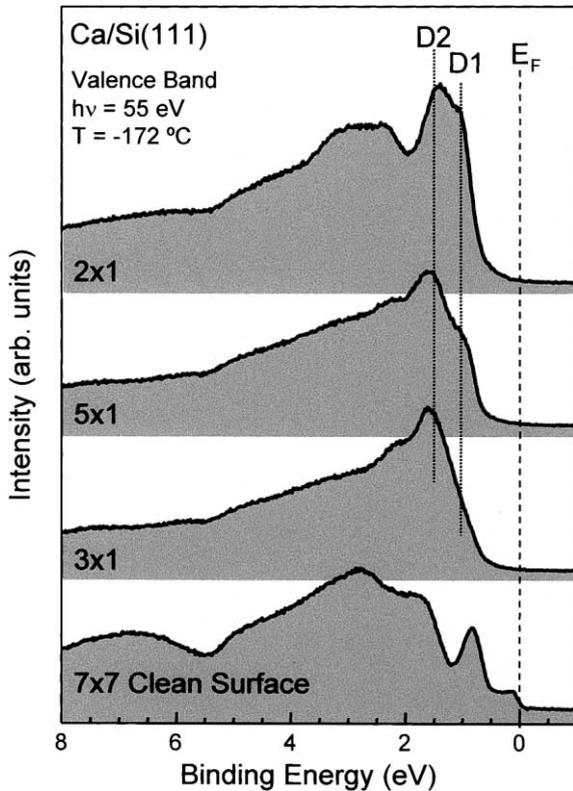


Fig. 9. Valence band spectra obtained from the 2×1 , 5×1 , and 3×1 phases of Ca on Si(111) and from the clean Si(111)-(7×7) surface. At least two surface states can be clearly observed in the data, which are labeled D1 and D2.

spectra again suggests that a massive rearrangement of Si atoms is unlikely. We detect two main surface state peaks that are labeled D1 and D2. The main feature D2 for all phases is a peak located at ~ 1.6 eV below the Fermi level, which increases slightly in intensity as the Ca coverage increases. The other surface state D1 increases dramatically in intensity as the Ca coverage increases. The D1 surface state therefore most likely corresponds to the back-bonds between the Ca and surface Si atoms, whereas D2 arises from Si–Si back-bonds between the first and second Si layers in the reconstructions. An interesting result is the lack of emission near the Fermi level for all phases, which is inconsistent with the predicted metallic behavior of the HCC model for the 3×1 phase. In the following section we propose that this result,

taken together with the STM observation of a $2a$ corrugation along the rows not present in diffraction studies, indicates that the 3×1 phase may be a 1D correlated insulator [18].

5. Discussion

A model for the metal-induced 3×1 phase was recently proposed based on diffraction data [4,5], where the metal atoms are assumed to sit in channels formed by neighboring Si honeycomb chains. The Si chains are 5- and 6-fold rings that have joined to form a chain with Si double bonds (see center region of Fig. 10). This HCC model has been found to be much more energetically favorable than previously proposed models and is consistent with STM and PES results [6,7]. Our STM data for the Ca/Si(111)- 3×1 surface is similar to that observed for the alkali metals and therefore suggests that the HCC model is also applicable to this system. The interesting development for Ca is the higher coverage odd-order phases (5×1 , 7×1 , etc.) which culminate in a 2×1 phase at 0.5

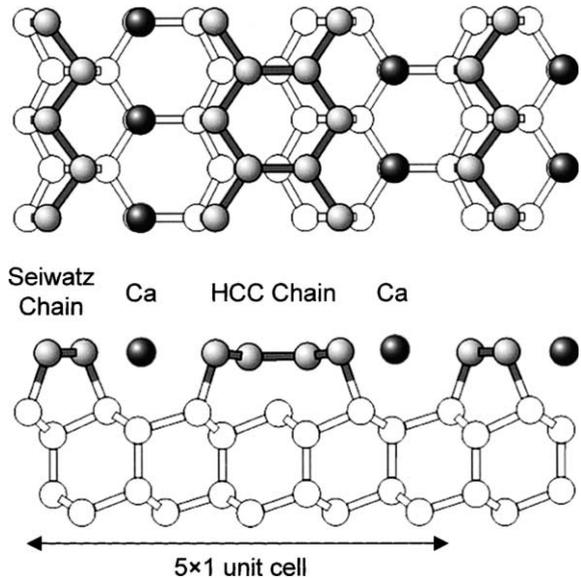


Fig. 10. Structural model for the intermediate 5×1 phase that incorporates double-bonded Si chains from the HCC 3×1 model and Seiwatz chains from our proposed 2×1 model.

ML. Because STM data show that the 3×1 rows may coexist with 5×1 and 7×1 rows, it appears that the higher coverage phases must incorporate Si subunits that are similar in nature to the Si HCC chains. Our RHEED and valence band PES results also support this conclusion.

In order to determine the structure of the odd-order phases, it is necessary to propose a model for the completion 2×1 phase. The odd-order phases can then be considered a mixture of the structural units found for the endpoint 2×1 and 3×1 phases. For example, a 5×1 unit cell would incorporate one 2×1 and one 3×1 unit cell, whereas a 7×1 unit cell would incorporate two 2×1 units and one 3×1 unit cell. One of the simplest possible models for the 2×1 phase incorporates Si chains composed of 5-fold rings, i.e. Seiwatz chains, where Ca sits in the channels between the Si chains. A 5×1 unit cell would then consist of one Seiwatz chain (or 2×1 structural unit) and one HCC chain (or 3×1 structural unit), as shown in Fig. 10. The Ca atoms are then located at T4 sites in the channels between the two types of Si chains. To form higher-order reconstructions, the proportion of Seiwatz chains is increased, e.g. the 7×1 unit cell consists of two Seiwatz chains and only one HCC chain. The Seiwatz chains then cover the surface at the completion 2×1 phase.

To test this model theoretically, we have calculated the absolute surface energies of the three simplest phases (3×1 , 5×1 , and 2×1) using the first-principles methods described above. Since the Ca coverage varies between these phases, we show in Fig. 11 each surface energy, $\gamma(\mu_{\text{Ca}})$, as a function of the Ca chemical potential, μ_{Ca} . Thermodynamics places an upper bound on the chemical potential of $\mu_{\text{Ca}} \leq \mu_{\text{Ca}}^{\text{bulk}}$, the energy per atom in bulk fcc Ca. This limiting value corresponds physically to saturation Ca coverage. Fig. 11 shows that for μ_{Ca} within 2.6 eV of this limit, the 2×1 Seiwatz-chain phase at $1/2$ ML coverage is energetically preferred. For values of μ_{Ca} less than about 3 eV below $\mu_{\text{Ca}}^{\text{bulk}}$, the 3×1 HCC reconstruction at $1/3$ ML coverage is the most stable phase. Between these stable endpoint phases, we also find a small window in which the 5×1 HCC + Seiwatz-chain phase at $2/5$ ML coverage is most stable.

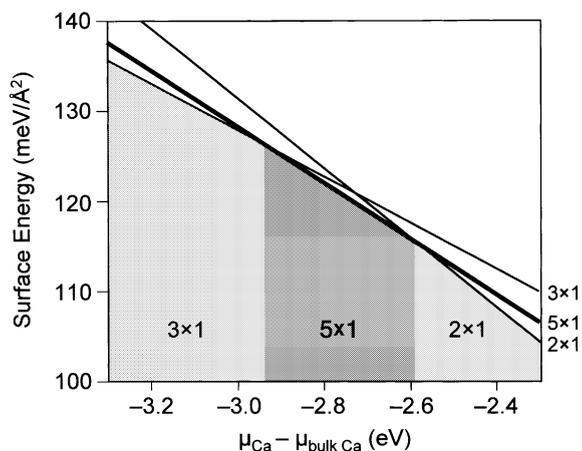


Fig. 11. First-principles theoretical surface energies for the 3×1 , 5×1 , and 2×1 phases, based on our proposed structural models. The surface energies are plotted as a function of Ca chemical potential, for thermodynamically allowed values within several eVs of the bulk energy per atom. Regions of stability for each of the three phases are shown as shaded areas.

The experimental implication of this result is that for a fixed coverage of $2/5$ ML, there is a range of values for the Ca chemical potential in which the system will not phase separate (at $T = 0$) into 2×1 and 3×1 domains, but will instead lower its energy by forming the pure 5×1 phase. At finite temperatures, however, entropic contributions to the free energy from intermixing may preempt the formation of large regions of the pure 5×1 phase. All of these findings are consistent with our experimental observations and lend strong support to our proposed structural model.

To test the validity of our proposed models, we have simulated constant-current STM images using the method described above. The insets in Fig. 4(a) and (b) show the theoretical filled and empty state images for a 5×1 unit cell, obtained by integrating the local-state density over a 2 eV energy range for both biases. The simulated images qualitatively confirm our proposed model. In the filled states, the dark trenches correspond to the double-bonded Si atoms of the HCC chains, whereas the bright stripes of the 5×1 unit cells each represent two Ca rows and one Seiwatz chain. Note that the resolution of the experimental STM images is not sufficient to distinctly show the $1a$

corrugations within these striped regions. In the empty states, the wider dark trenches are again the double-bonded Si atoms of the HCC chains, but at this bias voltage the Seiwatz chains also appear dark. The narrow bright stripes now correspond to the individual Ca rows, where two rows are present within each 5×1 unit cell. The lateral positions of these rows show relatively good agreement between the theoretical and experimental images. With regard to the STM data, our proposed model therefore appears consistent with observations of the higher coverage, odd-order phases.

Our proposed structural model can also be tested by calculating the predicted surface core-level shifts, and comparing with the experimental data. This comparison is made in Figs. 7 and 8, where the surface core-level shifts for all the atoms in our models are presented directly below the photoemission data. Both the IST and FST energies are shown.

For the simpler 2×1 phase, the agreement between the experimental data and the calculations is excellent. Moreover, because the calculated band structure for this phase is insulating, core-hole screening effects are small and the IST and FST shifts appear similar for all atoms. The calculated shifts in Fig. 7 fall into three ranges: (1) atoms a and d (≈ -0.45 eV), (2) atoms f , g , and h (close to bulk), and (3) atom j ($+0.25$ eV). The two Ca valence electrons are donated to Si orbitals located on atoms a and d and so these two core levels are shifted to lower binding energies. We therefore propose that the S2 component arises from atoms a and d in the Seiwatz chains. This component of the core-level spectrum increases in intensity as the Ca coverage increases, as expected. Atoms f , g , and h are all in a bulk-like environment and thus exhibit very small shifts relative to the bulk, making them unresolvable in the core-level decomposition. Lastly, atom j is located below the Ca atom in the channel. Based on simple atom counting, its intensity should be approximately half the combined intensity from atoms a and d , and should be suppressed further due to the short mean free path of the photoelectrons at these kinetic energies (~ 0.3 nm). It is then natural to associate the S1 component with atom j .

For the 3×1 phase, the comparison between theory and experiment is more problematic, in part because there are significant differences between the calculated IST and FST shifts. First, the FST core levels show an overall ~ 0.2 eV shift to lower binding energies relative to the IST levels. Second, the shift to lower binding energy for atoms b and c in particular is very large, nearly 0.5 eV. The overall shift is due to core-hole screening that is non-site-specific, as expected for a metallic system. The additional large screening found for atoms b and c can be traced to the partially occupied surface state denoted S_1^- in Ref. [6]. This state is a linear combination of orbitals on b and c . Thus, a core hole in either of these atoms will pull the S_1^- state closer to the Fermi level, leading to a large change in screening similar to that found in Si(001) [13]. We caution that neither IST nor FST can be completely justified for this phase, because the photoemission results in Fig. 9 show that the 3×1 phase is insulating.

The IST and FST shifts for the 3×1 phase can be roughly divided into three groups: (1) atom a , (2) atoms b – i , excluding g , and (3) atoms g and j . We again tentatively assign atom a in group 1 to the S2 component, in structural analogy to the 2×1 phase. Due to the large spread of energies in group 2, however, it is possible that contributions from atoms d (as would be expected) and h also contribute to S2. The second group of atoms has an average shift (IST and FST) close to the bulk, and is not identified with a core-level peak in any straightforward manner. The third group of atoms (g, j) is assigned to the S1 peak, where atom j is again analogous to the 2×1 phase. As mentioned earlier, this assignment is in disagreement with Kang et al., [7] who assigned the S1 component for Na to the double-bonded Si atoms labeled b and c .

We now turn our attention to the possibility that the 3×1 phase is a correlated insulator. The one-electron band structure for the 3×1 HCC model is insulating for alkali adsorbates, and so the addition of one more electron from an alkaline earth adsorbate must, within the one-electron description, result in a metallic band structure. This prediction is in disagreement with our angle-integrated valence band spectra. One question is whether the 3×1 reconstruction could in fact be

3×2 , which could result in an insulating surface. Our STM images show weak 3×2 ordering in both the filled and empty states (see Figs. 2 and 4), but our diffraction studies do not indicate any evidence for 3×2 ordering. It should be noted, however, that other work has reported weak half-order streaks for Yb, Sm, and Ca [8,9,15]. We believe that if the 3×2 ordering is structural in nature, then it is a minor perturbation of the HCC model and does not fully explain the surface's insulating behavior.

We therefore propose that the local doubling along the 3×1 rows is primarily of electronic, rather than structural, origin. Analogous behavior has been observed previously in the 2D systems of Pb/Ge(111) [19] and Sn/Ge(111) [20], wherein a number of mechanisms have been proposed to explain their unusual electronic/structural properties, including charge-density waves, dynamical lattice fluctuations [21], and spin (magnetic) ordering. One possibility is that the Ca/Si(111) system may exhibit strong electron correlations because of its quasi-1D structure. We are currently working on calculations and planning further experiments to address this possibility. It should be noted that for the related Ba/Si(111) system, there are in fact preliminary angle-resolved photoemission results suggesting that its 3×1 phase is a 1D Mott insulator [22].

6. Summary

In summary, the Ca/Si(111) system forms a series of odd-order $n \times 1$ ($n = 3, 5, 7, \dots$) reconstructions which culminate with a 2×1 phase at 0.5 ML. We have proposed the HCC model for the lower coverage 3×1 phase and a new Seiwatz chain model for the higher coverage 2×1 phase. The intermediate odd-order reconstructions are then formed by taking the appropriate combinations of the HCC and Seiwatz Si chains, e.g. a 5×1 unit cell incorporates one HCC and one Seiwatz chain. Calculated surface energies based on this model correctly predict that the 3×1 , 5×1 , and 2×1 phases each appear as stable phases for increasing Ca coverage. In addition, simulated STM images of the 5×1 phase are in

excellent agreement with experiment. Calculated IST and FST core-level shifts of the 2×1 phase agree quite well with experimental values, where Ca-bonded atoms are assigned to the prominent lower binding energy S2 peak. The 3×1 phase is more complex, however, and assignment of the calculated shifts is not as straightforward, although we believe the Ca-bonded atoms are still associated with the low binding energy component. It should be noted that valence band spectra indicate insulating behavior for all of the Ca-induced phases. This result is consistent with our proposed 2×1 model, but not with the band structure description of the 3×1 HCC model, indicating that further work is necessary to explain this insulating behavior.

Acknowledgements

This work was supported by NSF, DOE, the Research Corporation, and ONR. Computational work was supported by a grant of HPC time at the DoD Major Shared Resource Centers ARL, ASC, ERDC, and NAVO. J.A. Carlisle would like to thank Dr. Tom Miller and Dr. T.-C. Chiang (University of Illinois) for use of their photoemission endstation at the SRC. S.C. Erwin acknowledges helpful conversations with Dr. S.H. Lee and Prof. Dr. K. Horn of the Fritz Haber Institute (Berlin).

References

- [1] S. Hasegawa, M. Maruyama, Y. Hirata, D. Abe, H. Nakashima, Surf. Sci. 405 (1998) L503.
- [2] D. Jeon, T. Hashizume, T. Sakurai, R.F. Willis, Phys. Rev. Lett. 69 (1992) 1419.
- [3] K.J. Wan, X.F. Lin, J. Nogami, Phys. Rev. B 46 (1992) 13635.
- [4] C. Collazo-Davila, D. Grozea, L.D. Marks, Phys. Rev. Lett. 80 (1998) 1678.
- [5] L. Lottermoser, et al., Phys. Rev. Lett. 80 (1998) 3980.
- [6] S.C. Erwin, H.H. Weitering, Phys. Rev. Lett. 81 (1998) 2296.
- [7] M.-H. Kang, J.-H. Kang, S. Jeong, Phys. Rev. B 58 (1998) R13359.
- [8] C. Wigren, J.N. Andersen, R. Nyholm, U.O. Karlsson, J. Nogami, A.A. Baski, C.F. Quate, Phys. Rev. B 47 (1993) 9663.

- [9] C. Wigren, J.N. Andersen, R. Nyholm, M. Göthelid, M. Hammar, C. Törnevik, U.O. Karlsson, *Phys. Rev. B* 48 (1993) 11014.
- [10] B. Dardel, D. Malterre, M. Grioni, P. Weibel, Y. Baer, F. Levy, *Phys. Rev. Lett.* 67 (1991) 3144.
- [11] J.P. Perdew, K. Burke, M. Ernzerhof, *Phys. Rev. Lett.* 77 (1996) 3865.
- [12] M. Bockstedte, A. Kley, J. Neugebauer, M. Scheffler, *Comput. Phys. Commun.* 107 (1997) 187.
- [13] E. Pehlke, M. Scheffler, *Phys. Rev. Lett.* 71 (1993) 2338.
- [14] O. Kubo, A.A. Saranin, A.V. Zotov, J.-T. Ryu, H. Tani, T. Harada, M. Katayama, V.G. Lifshits, K. Oura, *Surf. Sci.* 415 (1998) L971.
- [15] A.A. Saranin, V.G. Lifshits, K.V. Ignatovich, H. Bethge, R. Kayser, H. Goldbach, A. Klust, J. Wollschläger, M. Henzler, *Surf. Sci.* 448 (2000) 87.
- [16] J.C. Woicik, P. Pianetta, T. Kendelewicz, *Phys. Rev. B* 40 (1989) 12463.
- [17] T. Okuda, et al., *Surf. Sci.* 321 (1994) 105.
- [18] J.D. Denlinger, G.H. Gweon, J.W. Allen, C.G. Olson, *Phys. Rev. Lett.* 82 (1999) 2540.
- [19] J.M. Carpinelli, H.H. Weitering, E.W. Plummer, R. Stumpf, *Nature* 381 (1996) 398.
- [20] J.M. Carpinelli, H.H. Weitering, M. Bartkowiak, R. Stumpf, E.W. Plummer, *Phys. Rev. Lett.* 79 (1997) 2859.
- [21] J. Avila, A. Mascaraque, E.G. Michel, M.C. Asensio, G. LeLay, J. Ortega, R. Perez, F. Flores, *Phys. Rev. Lett.* 82 (1999) 442.
- [22] J. Schaefer and E.L. Rotenberg, private communication.
- [23] S.H. Lee, M.H. Kang, personal communication.
- [24] Y. Qi, K. Sakai, H. Murakami, R. Aoki, T. Ito, *Thin Solid Films* 366 (2000) 77.